RSC Advances

ROYAL SOCIETY OF CHEMISTRY

www.rsc.org/advances

Hydrothermal synthesis and tribological properties of FeS_2 (pyrite)/reduced graphene oxide heterojunction

Mingsuo Zhang, BeiBei Chen, Hua Tang, Guogang Tang, Changsheng Li*, Lin Chen, Hongmei Zhang, Qing Zhang

Abstract: FeS_2 (pyrite)/reduced graphene oxide (FeS_2/RGO) heterojunction was synthesized by a facile and effective hydrothermal method. X-ray diffraction proved the high purity of the as-prepared product, both the scanning electron microscopy and transmission electron microscopy showed that FeS_2 particles were well distributed on RGO nanosheets with controlled size and morphology. The performance of the FeS_2/RGO composites as lubricating oil additive were investigated on the ball-plate tribotester. The results indicated that FeS_2/RGO could improve the load-carrying capacity dramatically, as well as the friction-reduction and anti-wear properties of the paraffin oil. In addition, higher GO content is beneficial to improve the lubrication properties of FeS_2/RGO composites. The excellent lubrication performance of FeS_2/RGO composites can be attributed to the unique layered structure of FeS_2 and RGO.

Key words: FeS_2; Reduced graphene oxide; Heterojunction; Lubrication additive; Tribological properties

1. Introduction

Graphene, an exciting new material with impressive one-atom-thick sheets of carbon atoms, has been investigated widely because of its unique thermal,[1] electrical [2] and mechanical properties.[3] It also shows outstanding optical properties such as high conductivities and transparency.[4] These excellent properties make it a good candidate for various applications such as nanoelectronics,[5] sensors,[6] composites[7] and supercapacitors.[8] Several methods have been developed to synthesize graphene, including epitaxial growth,[9] micromechanical exfoliation of graphite,[1] chemical vapor[10] and thermal or chemical reduction of graphite oxide (GO),[11] etc. Based on the unique properties of graphene, considerable efforts have been made to incorporate graphene into transition metal oxides or sulfides materials (Fe_3O_4, Co_3O_4, MoS_2 and FeS_2).[12-15] Nevertheless, few reports have been focused on the

tribological performance of the aforementioned graphene-based composites.

FeS_2 (pyrite), as an important member of transition metal sulfides, has a high optical absorption coefficient ($\alpha = 6\times10^5 cm^{-1}$), a narrow band gap of 0.95 eV, and an excellent optical, electrochemical and magnetic properties, which make it have a potential application in the fields of photovoltaic devices[16] and lithium-ion batteries.[17] At present, several efforts have been made in the syntheses and characterizations of FeS_2. Cabán-Acevedo et al.[18] studied the single-crystalline cubic iron pyrite nanowires synthesized via thermal sulfidation of a steel substrate. The pyrite nanowires have diameters of 4-10 nm and lengths greater than 2 μm. Hsiao et al.[19] synthesized the pure pyrite nanocrystals (NCs) with commonly used precursors via a simple, economical route. These pyrite NCs have a band gap of around ~1.1 eV with dimensions around ~14 to ~18. Puthussery et al.[20] prepared phase-pure, single-crystalline, and well-dispersed colloidal FeS_2 nanocrystals by a simple hot-injection route in octadecylamine.

Graphene-based composites witnesses rapid progress in the field of tribology in recent years due to their significant improvements in the mechanical and physical properties. For example, Zhang et al.[21] successfully synthesized reduced graphene oxide/Cu nanocomposites by a facile and effective chemical reduction method and showed improved wear resistance and load-carrying capacity than those in the oil with RGO nanosheets. Mo et al.[22] produced the chemically-modified reduced graphene oxide/polyacrylonitrile composites and studied their tribological performance. They claimed that the nanocomposite showed strong potential as a lubricant for industrial application due to their desirable thermal and tribological properties. The results from Hvizdš et al.[23] displayed enhanced friction and anti-wear performance of the Si_3N_4/graphene nanocomposites. However, there are few efforts devoted to the production of FeS_2/graphene composites. It is well known that FeS_2 constitutes a characteristic layered structure consisting of covalently bound S-M-S trilayers in analogy to MoS_2, which is particularly important for solid lubrication or as an additive for lubricating oils. In addition, FeS_2 (pyrite) has more abundant source, lower cost and better environmental compatibility when compared to many other lubricating oil additives such as MoS_2 and Cu, which make it very attractive among the inexpensive, earth-abundant candidate solar materials that have the potential to satisfy the annual worldwide energy demand[24]. At present, more efforts are devoted to the study of the lubrication performance of MoS_2[25-26]. However, it is a great pity that there are few reports on the tribological study of FeS_2. Therefore,

FeS_2/RGO is extremely promising as lubricant additives to improve the tribological properties of base oils.

Herein, we reported a facile hydrothermal method in the synthesis of FeS_2/RGO composites. The p/n heterojunction in FeS_2/RGO could be clearly observed (Scheme 1).[27] The tribological performance of the as-obtained FeS_2/RGO composites as base oil additive for lubrication was investigated and compared with pure RGO and FeS_2. To the best of our knowledge, this is the first report on the application of FeS_2/RGO composites as an oil-base lubricant additive.

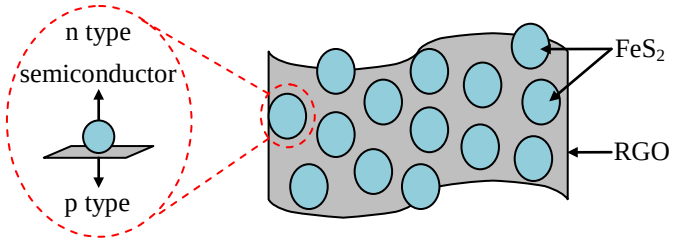

Scheme 1 The model of FeS_2/RGO heterojunction

2. Experimental

2.1 Synthesis of FeS_2 (pyrite)/RGO composites

GO was prepared by sophisticated Hummers method.[28] FeS_2 (pyrite)/RGO composites were synthesized using a hydrothermal process. Different concentrations of GO (0.10 g, 0.15 g and 0.20 g) were added together with 15 ml of distilled water under ultrasonication for 1 h, respectively. Then, 0.2 g iron chloride ($FeCl_2 \cdot 4H_2O$) was dissolved in 5 mL of distilled water, followed by addition of 0.3 g Polyvinylpyrrolidone (PVP) and stirring evenly. After completely dissolved, 5 ml sodium hydroxide (NaOH, 0.75 M) solution was added in the above solution. Then, 0.2 g sulfur powder (S) was added. Afterwards the above mentioned GO solution was added in the mixture solution with magnetic stirring for 0.5 h. Finally, the solution was transferred to a Teflon-lined autoclave (100 ml) and placed in an electric oven heated at 200℃ for 24 h. After the hydrothermal process, the as-prepared product was washed with distilled water and ethanol for several times and then dried in a vacuum oven at 60℃ for 8 h. Finally, black powders were obtained. For comparison, RGO nanosheets were prepared at the same condition without the addition of $FeCl_2 \cdot 4H_2O$ and sulfur powder. FeS_2 (pyrite) particles were synthesized following the same procedure without the addition of GO. The as-prepared sample names of FeS_2/RGO composites

are shown in Table 1.

Table 1 Sample names of FeS_2/RGO composites

Contents of GO/g	0.10	0.15	0.20
sample	FeS_2/RGO-A	FeS_2/RGO-B	FeS_2/RGO-C

2.2 Characterization

The crystallographic structure of the materials was determined by XRD measurement with a D8ADVANCE X-ray diffractometer (Bruker Corporation, Germany) equipped with a Cu Kα source in the range of 10-80° (λ = 0.1546 nm). The morphologies and particle sizes were characterized by scanning electron microscopy (SEM, JSM-7001F, JEOL) and transmission electron microscopy (TEM, JEM-2100, JEOL). Raman spectra was performed on the GO and FeS_2/RGO using a Renishaw inVia spectrometer with an excitation laser of 532 nm in wavelength.

2.3 Tribological measurement

The as-prepared FeS_2/RGO composites were added to the base oil liquid paraffin by mass fraction of 1 %, 3 %, 5 % and 7 %. RGO nanosheets and FeS_2 particles were processed by the same procedure. Solid powders were uniformly dispersed in the base oil with Ultrasonic generator and formulated into turbid liquid samples. Tribological properties of the base oil and mixed oil samples containing different mass fractions of additives were studied with a universal micro-tribotester (UMT-2, Center for Tribology Inc, USA). In order to evaluate the stability of the oil solution at various temperatures, 7 w.t.% FeS_2/RGO-C was dissolved in five glass bottles, respectively. After sonication for about 30 min, the oil blend was heated up from 20 to 160℃ and maintained at each temperature for about 60 min. In addition, the variation in the coefficient of friction under different loads and speeds were also investigated. The friction experiment was measured using ball on disc friction at a speed of 100-400 r/min loading at 6-30 N under room temperature for 10 min. The stainless steel ball with a diameter of 3 mm and a hardness of 62 HRC was made of 9Cr18 steel. The wear scar was measured by the VEECO WYKO NT1100 non-contact optical profile testing instrument.

3. Results and discussion

The XRD patterns of the as-prepared RGO, FeS_2 and FeS_2/RGO with different contents of GO are

displayed and compared in Fig. 1a. As can be seen clearly, the XRD pattern of the pure RGO has two broad peaks at about 2θ = 23° and 43° corresponding to the (002) inter-planar spacing of 0.4 nm and (100) that of 0.2 nm, respectively.[29] The (002) crystal plane is very broad, suggesting that the sample is very disorderedly along the stacking direction. The XRD pattern of FeS_2 exhibits high crystallinity and a typical cubic structure. All the diffraction peaks can be assigned to the crystalline FeS_2 according to the JCPDS card No. 71-0053. No other peaks for impurities were detected. We also observe that the FeS_2/RGO composites basically retain the layered crystallinity and the position of the diffraction peaks of FeS_2. However, it is worth noticing that the intensity of all the diffraction peaks of FeS_2 decrease with increasing RGO content in the composites, which indicates that the incorporation of the RGO considerably inhibits the growth of FeS_2 crystals in the composites. Additionally, the peaks of the RGO sheets could hardly be detected in the FeS_2/RGO composites, which can be attributed to shielding of the RGO peaks by FeS_2 particles anchored on the surface of RGO sheets and the relatively low diffraction intensity of graphene,[30] suggesting of less agglomeration for RGO sheets in composites. When the RGO content is high enough, the peak of RGO emerged (Fig. 1b). Fig. 1c shows the Energy-dispersive X-ray spectrometer (EDS) analysis of the FeS_2/RGO-C, which reveals that the composites consist of element Fe, S and C and no other element was observed. Furthermore, the quantification of the peaks shows that the atom ratio of Fe to S is about 1:2.18, which is very close to the stoichiometry of FeS_2.

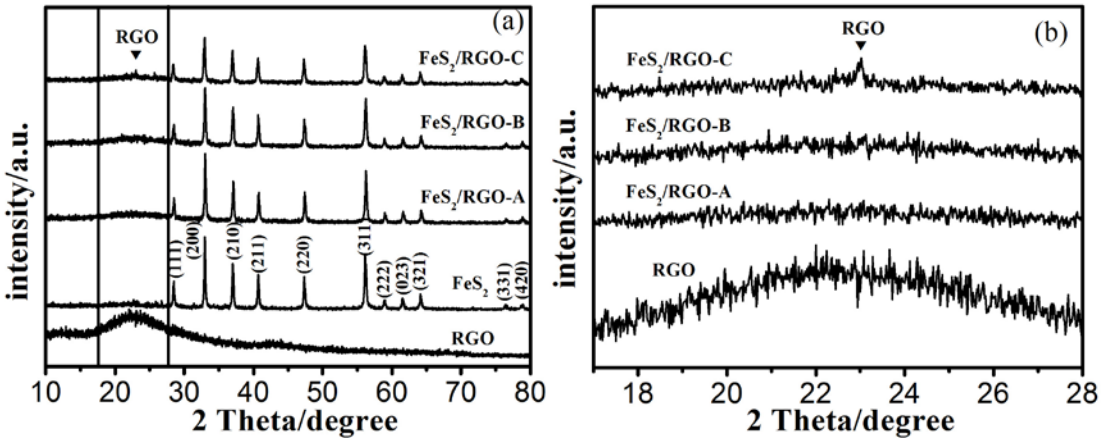

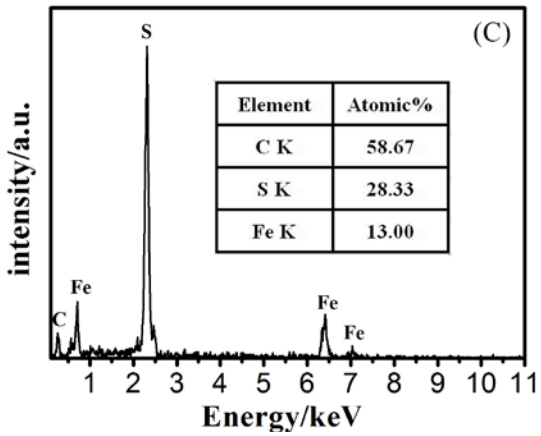

Fig. 1. (a) XRD patterns of RGO, FeS_2 , FeS_2/RGO-A, FeS_2/RGO-B and FeS_2/RGO-C; (b) High magnification XRD patterns of the pure RGO and FeS_2/RGO of the selected area in Fig. 1a; (c) EDS of FeS_2/RGO-C

Fig. 2 shows the Raman spectra of GO and FeS_2/RGO-C, respectively. It can be seen that both GO and FeS_2/RGO exhibite two broad bands at around 1360 cm^{-1} and 1585 cm^{-1}, which correspond to sp^3 (D band) and sp^2 (G band) hybridization carbon atoms, respectively.[31] The intensity of D band is stronger than that of G band and this indicates the presence of high density of defects and structural disorder in RGO.[32] Remarkably, the D:G intensity ratio of FeS_2/RGO increases compared to that of GO after reduction (from 0.94 to 1.08), suggesting the reduction process leads to the increase of disorder and defects of the RGO layers. Moreover, The Raman spectrum of FeS_2/RGO-C also shows three peaks at 340, 376 and 440cm^{-1}, which are ascribed to the S_2 libration (E_g), S-S in-phase stretch (A_g), and coupled libration and stretch (T_g) modes, respectively (inset of Fig.2).[33-34] No other peaks were observed, which was consistent with the XRD results. Based on the Raman spectroscopy results, we confirm that the FeS_2/RGO composites are composed of pure FeS_2 (pyrite) and RGO sheets.

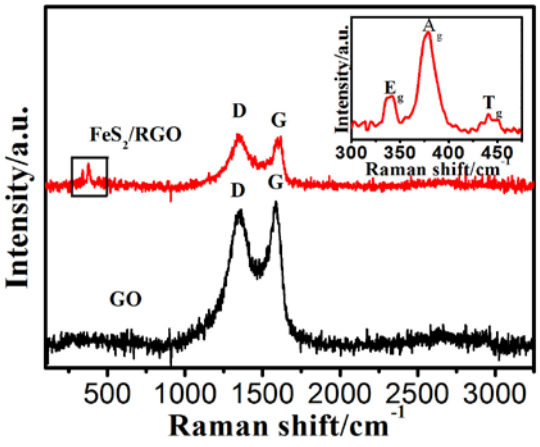

Fig. 2. Raman spectra of GO and FeS_2/RGO-C

The SEM images of FeS_2, FeS_2/RGO-A, FeS_2/RGO-B, and FeS_2/RGO-C are shown in Fig. 3. As clearly shown in Fig. 3a, the as-prepared FeS_2 has an octahedral-like shape with an average particle size of 350 nm. From the geometry of polyhedra, the octahedron is enclosed by {111} facets. Fig. 3b shows the high magnification SEM image of FeS_2 particles. It is observed that FeS_2 particles have relatively perfect octahedral shapes with sharp corners and edges and bounded by smooth surfaces. Fig. 3c-h show the SEM images of FeS_2/RGO composites prepared with different concentrations of GO (0.10, 0.15 and 0.20 g). Clear morphological and size changes can be observed with increasing GO concentration. When the concentration of GO was 0.10 g, the obtained FeS_2 exhibits octahedral shape with average particle size of 2000 nm (Fig. 3c). The surface is relatively rough (Fig. 3d). As the GO concentration is increased to 0.15 g (Fig. 4e and f), the FeS_2 particles are cubic-like in shape while their average particle size is estimated to be 1300 nm. A further increase of the GO concentration to 0.20 g gives rise to spherical-like morphology of the FeS_2 particles and their average particle size decreased about sixfold (~200 nm, as shown in Fig. 4g and h). From the above description, with the increase of the concentration of GO, the average particle size of FeS_2 particles not only decreased obviously but also the morphology of that gradually grew towards sphere. The possible reason is that FeS_2 crystals were wrapped by the RGO nanosheets during the synthesis, gradually preventing their further growth with the increase of the GO concentration, which is consistent with the above XRD results. These results indicate that GO plays a decisive role in controlling the size and morphology of the FeS_2 particles.

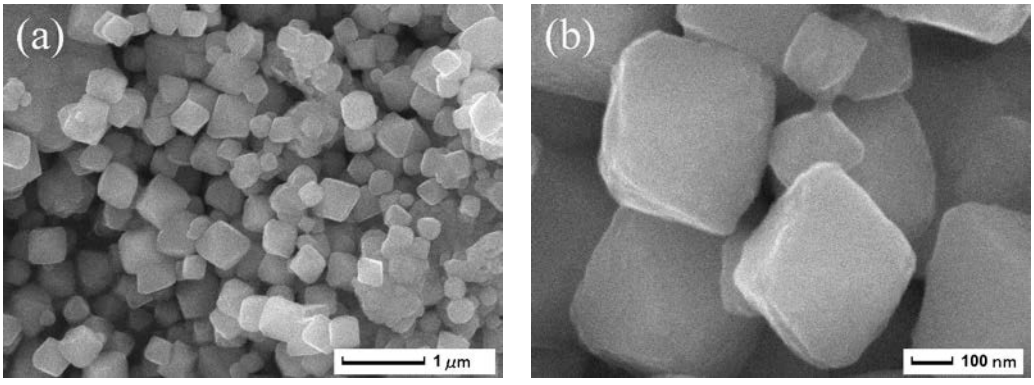

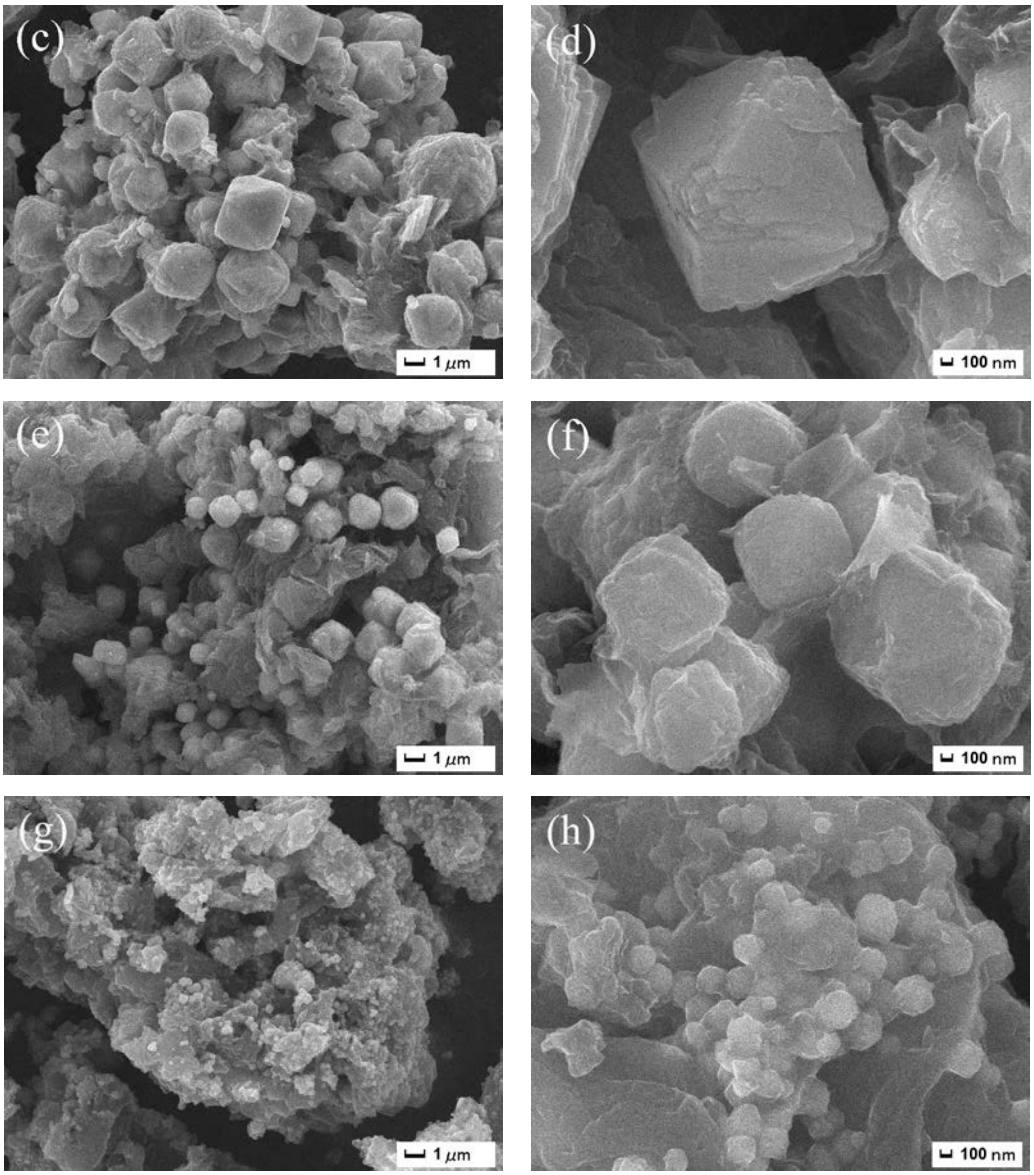

Fig. 3. SEM images of (a, b) FeS_2, (c, d) FeS_2/RGO-A, (e, f) FeS_2/RGO-B and (g, h) FeS_2/RGO-C

The morphology of the FeS_2/RGO-C was further characterized by TEM due to small particle size and spherical-like shape of FeS_2. It can be seen from Fig. 3a that the surfaces of FeS_2 are covered completely by successive and uniform RGO sheets, which indicates the formation of the FeS_2/RGO heterojunction. Meanwhile, the aggregation of FeS_2 was well prevented by the RGO sheets. Fig. 3b is the high-magnification TEM image. The profile of single FeS_2 particle can be clearly distinguished. In addition, it is also found that the surfaces of FeS_2 particles are fuzzy. The reason is that the surfaces of FeS_2 particles were covered by RGO nanosheets, which provides further evidence that the FeS_2/RGO heterojunction was formed in this work.

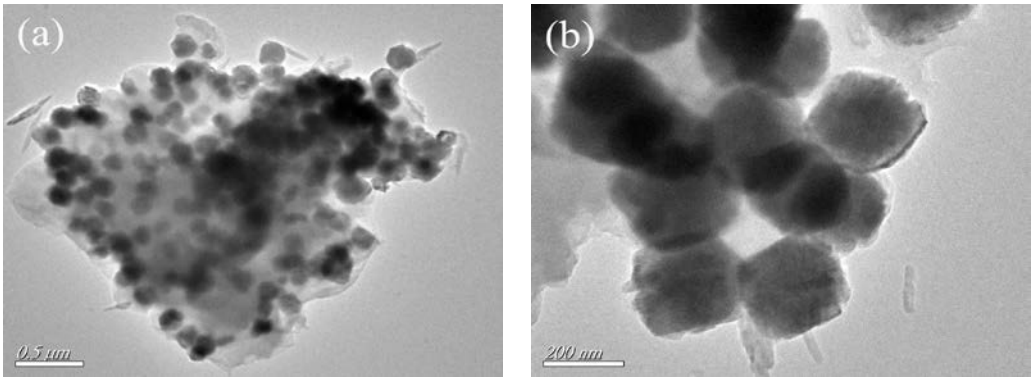

Fig. 4. (a) TEM image of FeS_2/RGO-C; (b) High-magnification TEM image of FeS_2/RGO-C

In order to investigate the variations of the friction coefficients with the different concentrations of various additives, the tribological performance of the oil with RGO, oil with FeS_2 and oil with FeS_2/RGO adding different contents of GO were tested under a load of 20 N for 10 min, respectively. All friction coefficients herein were evaluated as averages of three replicate tests for each experimental material under the same sliding conditions. The variation in friction coefficient values shown for each trial was very low and the relative error for the friction was below 10%. It can be seen from Fig .6 that the friction coefficients of friction pairs lubricated by various additives have a downward trend as a whole with increasing additive concentration except RGO, whose friction coefficient increases clearly when the concentration of RGO is over 5 w.t.%. The possible reason is that RGO is not able to disperse well in the paraffin oil with increasing the content of RGO because of its large specific surface area and specific surface energy, which lead to the formation of agglomerates. It also can be seen that the comprehensive tribological properties of the paraffin oil containing FeS_2/RGO were improved gradually with the increase of GO concentration in FeS_2/RGO. According to Spikes,[35] mechanical entrapment theory, friction and wear variations of the nanoparticles suspensions are related to the size, hardness, and deposition of nanoparticles on wear surfaces. Thus the size and morphology of FeS_2 particles in FeS_2/RGO composites play an important role in the lubricant regime. Further discussion is provided in Fig. 5b. It shows the variation of friction coefficients of the paraffin oil with the concentration of 7 w.t.% RGO, FeS_2, FeS_2/RGO-A, FeS_2/RGO-B and FeS_2/RGO-C under a condition of 20 N, 300r/min and 10 min. It can be found that the paraffin oil with FeS_2/RGO-C heterojunction gives a lower and more stable friction coefficient than others. At the end of friction and wear test, no precipitation of the additive was found. The excellent tribological performance of FeS_2/RGO-C heterojunction can be attributed to their small size and extremely thin laminated structure. Moreover, the presence of FeS_2 particles on RGO layers can act

as nanobearing between moving parts and can reduce the friction. The special-like shape makes them easily penetrate into the interface with paraffin oil and deposit a continuous protective film, so the performance of friction coefficient is more stable than others.

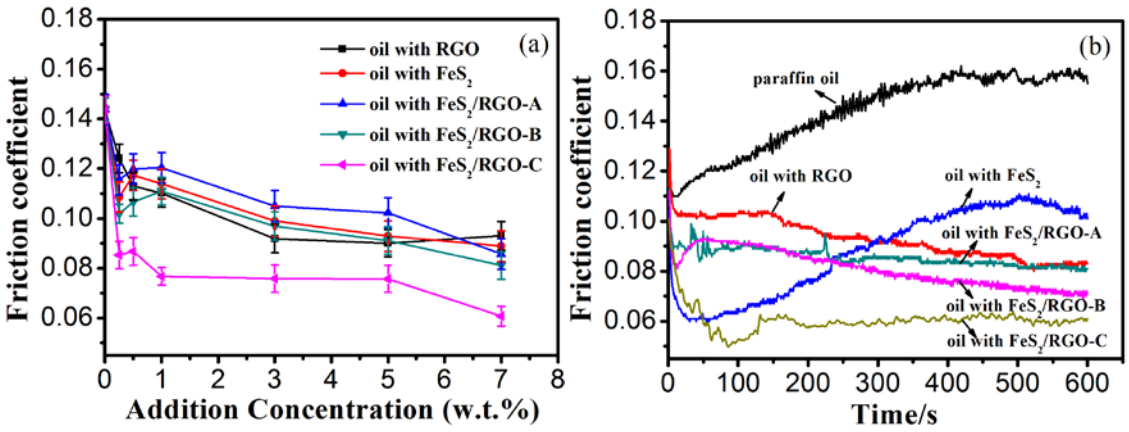

Fig. 5. (a) Variations in the friction coefficient with concentration of additives of RGO, FeS_2, FeS_2/RGO-A, FeS_2/RGO-B and FeS_2/RGO-C (20 N, 300r/min, 10 min); (b) Curves of friction reduction properties for 1) the paraffin oil, 2) oil with 7 w.t.% RGO, 3) oil with 7 w.t.% FeS_2, 4) oil with 7 w.t.% FeS_2/RGO-A, 5) oil with 7 w.t.% FeS_2/RGO-B, 6) oil with 7 w.t.% FeS_2/RGO-C

According to Qiu[36], lubricating effectiveness is not only affected by the amount of the additive, but also the temperature at contacting regions. It is well known that the dispersion stability of oil blend with solid powders has a great influence on the lubricant properties of oil. And the temperature is an important factor to affect the dispersion stability of oil blend. As an example of the oil blend with 7 w.t.% FeS_2/RGO, the stability of the blend at various temperatures has been investigated in Fig. 6. It was observed that the oil blend displayed good dispersion stability at the temperature from 20 to 120℃. But only the temperature reaches 160℃, there are a very little sediments and a supernatant can be observed, which may be caused by the intensification of Brownian motion because of high temperature. These results indicate that the oil blend can meet the requirement of stability under most of temperature conditions.

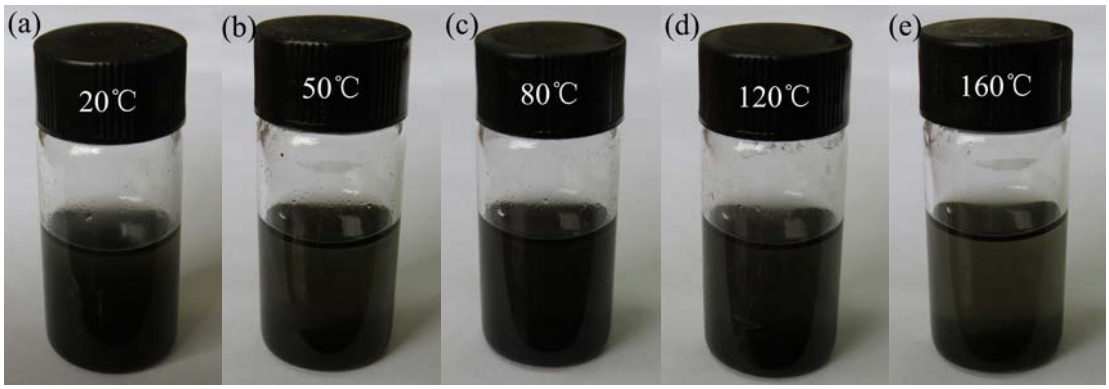

Fig. 6. Dispersion of 7 w.t.% FeS_2/RGO composites in base oil at various temperatures

To further evaluate the lubricating performance of oil solution with the extension of time, the test time of oil with 7 w.t.% FeS_2/RGO-C heterjunction was increased to 3h. And the variation of friction coefficient with sliding time has been shown in Fig. 7, it can be clearly seen that the friction coefficient nearly keeps 0.057 during the whole friction and wear process. And any sharp fluctuation has not been found. The result well suggests that the base oil containing 7 w.t.% FeS_2/RGO-C heterjunction still processes excellent friction-reducing property, even experiencing longer test time. In fact, according to the investigation of Ingolea et al[37], the precipitation of the additive did have an effect on tribological properties of the oil blend. But the precipitation scarcely could be observed at the end of the test, this might be ascribed to the constant agitation effect of friction counterpart during the test. Hence, the little precipitation of the additive did not obviously affect the friction coefficient of the oil blend according our test .

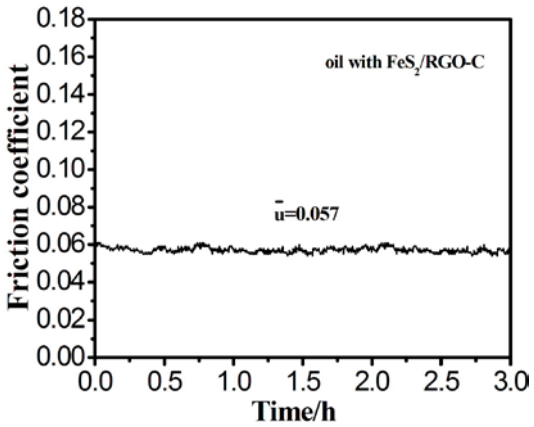

Fig. 7. Friction coefficient Curve of oil with 7 w.t.% FeS_2/RGO-C at applied load 20 N and sliding speed 300r/min

Fig. 8a and b show the variations of friction coefficient of 7 w.t.% FeS_2/RGO-C heterojunction as an additive of lubricant under different loads and sliding speeds, respectively. It can be seen that there is a tendency that the friction coefficient of FeS_2/RGO-C decreases firstly and then increases as the load or sliding speed increases. We can get the optimal load and sliding speed for friction performance at 10 N and 300 r/min. In a certain pressure range, FeS_2/RGO-C is delaminated easily at the contact zone with the load increased, which can decrease shearing stress and give a low friction coefficient. When the pressure is over 20 N, the friction coefficient increases due to the destruction of the protective film at the contact zone under high loads. The effect of sliding speeds on the friction coefficient of FeS_2/RGO-C is also discussed. It is well known that the thickness of oil film will increase with raising speed, which will decrease the contact of asperity between the rubbing surfaces, thereby the friction coefficient of the paraffin oil with 7 w.t.% FeS_2/RGO-C decreased firstly with increasing the sliding speed (Fig. 8b). While the friction coefficient has a slight increase when the velocity is more than 300 r/min. The possible reason is that the increase of sliding speed accelerated the degradation between the paraffin oil and additive due to increasing temperature at the contact zone, leading to increased friction coefficient.

A phenomenon can be seen that the curves 1, 2 and 4 have higher noise than the curve 3 in Fig. 8a and b. From Fig. 8a, when the applied load was 20N, FeS_2/RGO-C with small size can easily enter a macroscopic sliding contact and a continuous protective film was formed during the friction and wear test,[38] which showed high load-carrying capacity and therefore a relatively low noise. When the applied load was smaller than 20 N, FeS_2/RGO-C heterjunction cannot be compacted on the worn surface to mend wear scar, so the protective film was not formed. On the contrary, if the applied load is too high, the protective film will be destructed, finally leading to high noise. From Fig. 8b, when the sliding speed was small,[39] the viscosity of the oil blend was comparatively high because of low temperature at contacting regions, which will lead to bad mobility of the oil and the friction resistance between friction pairs will increase. So the noise is high. However, as the sliding speed exceeded a critical value, the viscosity of the oil blend was very low because of high temperature at contacting regions and the oil film between the rubbing surfaces cannot be easily established, which lead to high noise. The test results indicate that the oil blend has suitable viscosity when the sliding speed is 300r/min.

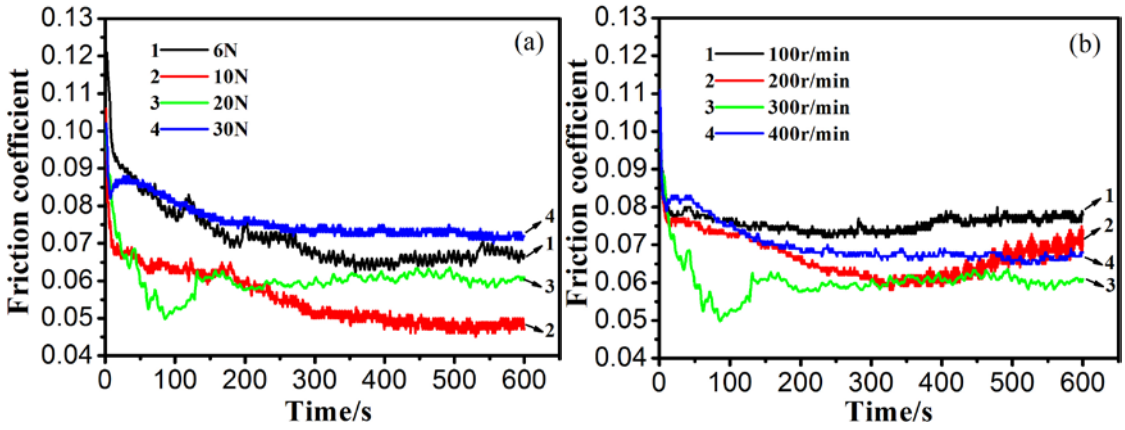

Fig. 8. (a) Curves of friction reduction properties of lubricant with 7 w.t.% FeS_2/RGO-C as an additive of lubricant under various load (300 r/min, 10 min); (b) Curves of friction reduction properties of lubricant with 7 w.t.% FeS_2/RGO-C as an additive of lubricant under various rotary speed (20 N, 10 min)

In order to investigate the anti-wear property of FeS_2/RGO as lubricant oil additives, the wear scars of plate after rubbing were tested by a VEECO WYKO NT1100 non-contact optical profile testing instrument. Fig. 9 illustrates wear scars of the paraffin oil, oil with FeS_2 and oil with FeS_2/RGO-C at 300 r/min under 20 N loads. Obviously, the grinding track for the base oil is composed of wide grooves and irregular pits along the sliding direction (Fig. 9a), whereas the one in Fig .9c is shallower than those in Fig .9a and b. From the images, the depth and width of wear scar of base oil with 7 w.t.% FeS_2 are about 3.5 μm and 360 μm, respectively, while those of base oil with 7 w.t.% FeS_2/RGO-C are about 1.3 μm and 310 μm. These results prove that the lubricant performance of FeS_2/RGO-C is better than that of the base oil and FeS_2.

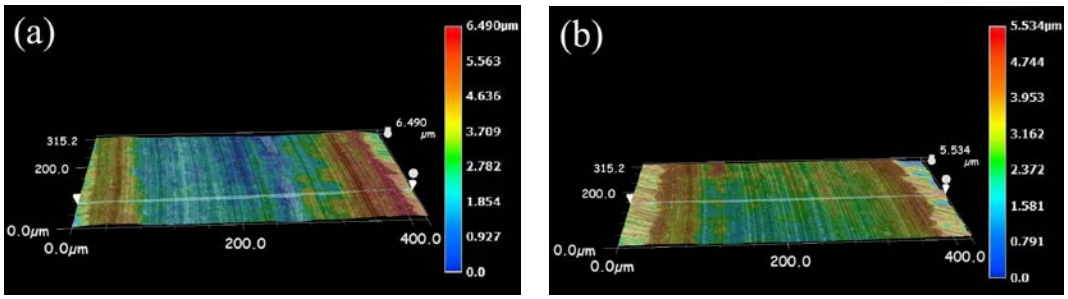

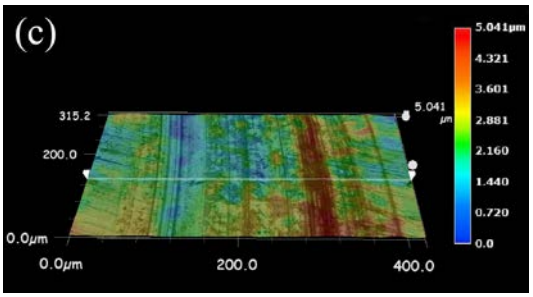

Fig. 9. Non-contact optical profile testing instrument images of the grinding tracks of (a) the paraffin oil, (b) the paraffin oil with 7 w.t.% FeS_2, (c) the paraffin oil with 7 w.t.% FeS_2/RGO-C at 300 r/min under 20 N loads for 10 min

In this work, FeS_2/RGO composites have shown a very low friction coefficient and good anti-wear ability under a certain condition. The tribological mechanism between the rubbing surfaces in base oil with FeS_2/RGO heterojunction is vividly proposed in Fig. 10. We propose the possible mechanism behind reducing friction in the case of FeS_2/RGO as additive in paraffin oil. When we add FeS_2/RGO to the base oil, FeS_2 as transition metal sulfides MS_2 was delaminated easily,[40] and the RGO can slide between the surfaces in the oil because of its geometry of planar. Therefore, FeS_2/RGO composites can fill up the microgaps of the rubbing surfaces, and form a continuous lubricating film on the metal substrate due to the stressed zones of traction/compression created by the high contact pressure. The FeS_2/RGO tribofilm could not only bear the load of the steel ball but also prevent the direct contact of two mating metal surfaces. Therefore, the friction coefficient of the oil with additive was decreased, and the anti-wear ability was improved. Although the FeS_2 and RGO can also form the corresponding tribology film in specific areas, the distribution of tribofilm is no-homogeneous resulting from their aggregation of the nanoparticles and nanosheets, leading to the higher friction coefficient.

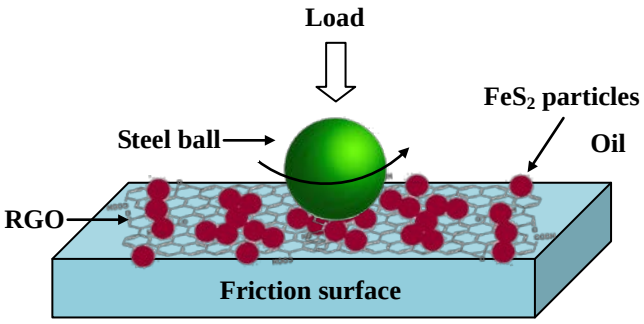

Fig. 10. Mechanism model of friction reduction and wear resistance between friction surfaces in the paraffin oil with FeS_2/RGO heterojunction

Conclusions

In summary, we have successfully synthesized FeS_2/RGO composites by a facile and effective hydrothermal method. The results indicated that the size of the FeS_2 particles gradually decreased from ~2000 nm to ~200 nm and the corresponding morphologies were changed from octahedral to sphere-like due to the incorporation of more GO content into FeS_2/RGO composites. In particular, the FeS_2/RGO-C composites deliver a heterojunction. The tribological measurements showed that FeS_2/RGO-C heterojunction by mixing with paraffin oil has better friction reduction and wear resistance properties compared with the base oil, oil with pure RGO and oil with FeS_2. Moreover, the tribological properties of the FeS_2/RGO composites were improved with increasing GO content. Formation of nanobearing between two rubbing surfaces plays a major role in reducing the friction and wear. The excellent performance of FeS_2/RGO composites on tribological properties of paraffin oil is attributed to the synergistic effects between layered FeS_2 and RGO.

Acknowledgement

This work was financially supported by National Natural Science Foundation of China (51275213, 51302112), the Jiangsu National Nature Science Foundation (BK2011534, BK2011480), the Jiangsu Industry-University-Research Jointinnovation Foundation (BY213065-05, BY213065-06) and a Project Funded by Priority Academic Program Development of Jiangsu Higher Education Institutions.

Notes and references

School of Materials Science and Engineering, Jiangsu University, Key Laboratory of high-end structural materials of Jiangsu Province, Zhenjiang, Jiangsu 212013, P.R. China. Fax: +86 511 8879 0268; Phone: +86 511 8879 0268; E-mail: lichangsheng@mail.ujs.edu.cn

[1] K. S. Novoselov, A. K. Geim, S. V. Morozov, D. Jiang, Y. Zhang, S. V. Dubonos, I. V. Grigorieva, A. A. Firsov, *Science*. 2004, **306**, 666.

[2] K. Kim, H.J. Park, B.C. Woo, K.J. Kim, G.T. Kim, W.S. Yun, *Nano Lett*. 2008, **8**, 3092.

[3] C. Lee, X.D. Wei, J.W. Kysar, J. Hone, *Science*. 2008, **321**, 385.

[4] R.R. Nair, P. Blake, A.N. Grigorenko, K.S. Novoselov, T.J. Booth, T. Stauber, N.M.R. Peres, A.K. Geim, *Science*. 2008, **320**, 1308.

[5] D.A. Areshkin, C.T. White, *Nano Lett*. 2007, **7**, 3253.

[6] Y.H. Zhang, Y.B. Chen, K.G. Zhou, C.H. Liu, J. Zeng, H.L. Zhang, Y. Peng, *Nanotechnology*. 2009, **20**, 185504.

[7] H. Tang, P.b. Gao, A. Xing, S. Tiana, Z.H. Bao, *RSC Adv*. 2014, **4**, 28421.

[8] C. Liu, Z. Yu, D. Neff, A. Zhamu, B.Z. Jang, *Nano Lett*. 2010, **10**, 4863.

[9] C. Berger, Z.M. Song, X.B. Li, X.S. Wu, N. Brown, C. Naud, D. Mayou, T.B. Li, J. Hass, A.N. Marchenkov, E.H. Conrad, P.N. First, W.A. de Heer, *Science*. 2006, **312**, 1191.

[10] X.S. Li, C.W. Magnuson, A. Venugopal, J.H. An, J.W. Suk, B.Y. Han, M. Borysiak, W.W. Cai, A. Velamakanni, Y.W. Zhu, L.F. Fu, E.M. Vogel, E. Voelkl, L. Colombo, R.S. Ruoff, *Nano Lett*. 2010, **10**, 4328.

[11] H. Zhang, X. Lv, Y. Li, Y. Wang, J. Li, *ACS Nano*. 2010, **4**, 380.

[12] C. Santhosh, P. Kollu, S. Doshi, M. Sharma, D. Bahadur, M.T. Vanchinathan, P. Saravanan, B.S. Kime, A.N. Grace, *RSC Adv*. 2014, **4**, 28300.

[13] C.C. Xiang, M. Li, M.J. Zhi, A. Manivannan, N.Q. Wu, *J. Power. Sources*. 2013, **226**, 65.

[14] K. Chang, W.X. Chen, *ACS Nano*. 2011, **5**, 4720.

[15] A. Moradi Golsheikh, N.M. Huang, H.N. Lim, C.H. Chia, I. Harrison, M.R. Muhamad, *Chem. Eng. J.* 2013, **218**, 276.

[16] C.W. Lin, D.Y. Wang, Y.T. Wang, C.C. Chen, Y.J. Yang, Y.F. Chen, Sol. Energ. *Mat. Sol. C.* 2011, **95**, 1107.

[17] X. Feng, X.M. He, W.H. Pu, C.Y. Jiang, C.R. Wan, *Ionics*. 2007, **13**, 375.

[18] M. Cabán-Acevedo, M.S. Faber, Y. Tan, R.J. Hamers, S. Jin, *Nano Lett*. 2012, **12**, 1977.

[19] S.C. Hsiao, C.M. Hsu, S.Y. Chen, Y.H. Perng, Y.L. Chueh, L.J. Chen, L.H. Chou, *Mater. Lett*. 2012, **75**, 152.

[20] J. Puthussery, S. Seefeld, N. Berry, M. Gibbs, M. Law, *J. Am. Chem. Soc*. 2011, **133**, 716.

[21] Y. Zhang, H. Tang, X.R. Ji, C.S. Li, L. Chen, D. Zhang, X.F. Yang, H.T. Zhang, *RSC Adv*. 2013, **3**, 26086.

[22] Y.F. Mo, M.L. Yang, Z.X. Lu, F.C. Huang, *Composites Part A*. 2013, **54**, 153.

[23] P. Hvizdš, J. Dusza, C. Balázsi, *J. Eur. Ceram. Soc*. 2013, **33**, 2359.

[24] C. Wadia, A.P. Alivisatos, D.M. Kammen, *Environ. Sci. Technol*. 2009, **43**, 2072.

[25] H.T. Yu, Y. Liu, S.L. Brock, *Inorg. Chem*. 2008, **47**, 1428.

[26] G.G. Tang, J. Zhang, C.C. Liu, D. Zhang, Y.Q. Wang, H. Tang, C.S. Li, *Ceram. Int*. 2014, **40**, 11575.

[27] S. Gilje, S. Han, M. Wang, K.L. Wang, R.B. Kaner, *Nano Lett*. 2007, **7**, 3394.

[28] C.M. Chen, Q.H. Yang, Y.G. Yang, W. Lv, Y.F. Wen, P.X. Hou, M.Z. Wang, H.M. Cheng, *Adv. Mater*. 2009, **21**, 3007.

[29] C. Wang, C. Feng, Y. Gao, X. Ma, Q. Wu, Z. Wang, *Chem. Eng. J*. 2011, **173**, 92.

[30] Y. Fan, H.T. Lu, J.H. Liu, C.P. Yang, Q.S. Jing, Y.X. Zhang, X.K. Yang, K.J. Huang, *Colloid. Surf. B*. 2011, **83**, 78.

[31] U.S. Schwarz, S. Komura, S.A. Safran, *Europhys*, 2000, **50**, 762.

[32] J. Lu, J.X. Yang, J. Wang, A. Lim, S. Wang, K.P. Loh, *ACS Nano*. 2009, **3**, 2367.

[33] Y. Golan, C. Drummond, J. Israelachvili, R. Tenne, *Wear*. 2000, **245**, 190.

[34] T. Kamegawa, D. Yamahana, H. Yamashita, *J. Phys. Chem. C*. 2010, **114**, 15049.

[35] F. Chiñas-Castillo, H.A. Spikes, *J. Tribol-T. Asme*. 2003, **125**, 552.

[36] S.Q. Qiu, Z.R. Zhou, J.X. Dong, G.X. Chen, *J. Tribol.* 2001, **123**, 441.

[37] S. Ingolea, A. Charanpahari, A. Kakadec, S.S. Umare, D.V. Bhatt, J. Menghani, *Wear.* 2013, **301**, 776.

[38] T. Luo, X.W. Wei, H.Y. Zhao, G.Y. Cai, X.Y. Zheng, *Ceram. Int*. 2014, **40**, 10103.

[39] M. Zhang, X.B. Wang, X.S. Fu, Y.Q. Xia, *Tribol. Int*. 2009, 42, 1029.

[40] A.K. Kleppe, A.P. Jephcoat, *Mineral. Mag.* 2004, **68**, 433.